JOURNAL OF MATERIALS SCIENCE 26 (1991) 2685–2693

The development of Fe–Al intermetallics

A. BAHADUR, O. N. MOHANTY
National Metallurgical Laboratory, Jamshedpur 831 007, India

The intermetallics based on aluminides have long been known for their excellent resistance to high-temperature oxidation. However, for use in structural components the poor ductility at ambient temperatures has always been felt as a stumbling block. Interest in these materials has been revived recently, after achieving some success in improving the ductility at ambient temperatures and creep at elevated temperatures in titanium aluminides. For the iron aluminides, too, similar methodologies have been attempted, namely alloying with elements such as titanium, boron, molybdenum, chromium, silicon and manganese, as well as grain refinement for improving high-temperature creep and room-temperature ductility. Raising the creep resistance close to 600 °C and improving the ambient-temperature ductility to around 6% have been the major immediate aims. Attempts are also being made to improve the high-temperature fatigue and creep properties in these materials, particularly by pushing the stability temperature of ordered DO_3 upwards. It is now visualized that once the above properties are achieved, the iron aluminides, particularly the types based on Fe_3Al, could offer themselves as excellent candidate materials for structural purposes. Their attractiveness also stems to a large extent from their low cost, as they contain only abundantly occurring materials. The present work examines two routes for introducing ductility in the Fe_3Al-based materials: one by ternary–quarternary additions and the other by grain refinement. Structural studies have been made on materials obtained through conventional casting as well as through rapid solidification with minor alloy additions. The results confirm that Fe_3Al-based alloys, even when air-melted, are amenable to a high degree of hot working and could be made to display improved ductility at room temperature by a careful control of the chemistry. Rapidly solidified ribbons also show reasonably good bonding during high-temperature compaction. Ordering in these alloys is not suppressed even by rapid solidification.

1. Introduction

Excellent high-temperature strength properties of intermetallics, occurring in relatively narrow compositional ranges around simple stoichiometric ratios, have long been recognized and are attributed to long-range ordered superlattices. Aluminides represent an important group of materials in this class.

The structural use of ordered intermetallic compounds based on aluminides has not materialized commercially because of the brittleness at ambient temperature and rather poor creep properties. Efforts to improve these properties through the 1960s did not meet with much success and interest in structural aluminides therefore waned. A marked revival has, however, been witnessed particularly with the success in improving creep and ductility properties in titanium and nickel-aluminides through grain refinement and alloying [1–15].

The aluminides of nickel, titanium and iron contain sufficient amounts of aluminium to form thin, adherent, protective films of Al_2O_3 in an oxidizing environment, which impart resistance to further oxidation and corrosion (particularly in a sulphurated atmosphere) even at high temperature. Their low density, relatively high melting points and good high-temperature strength [16–18] are other attractive properties. Some general characteristics of these materials are given in Table I [19].

Among the aluminides, the ones based on Fe–Al have a special attractiveness in that they are the least expensive. Here, both Fe_3Al and FeAl compounds have engaged the attention of researchers. However, Fe_3Al is believed to possess greater potential owing to its relatively higher ductility.

Considerable efforts have recently been channelled into introducing satisfactory high-temperature creep properties and improved ambient-temperature ductility in Fe_3Al through alloying with elements such as boron [20–22], titanium [23, 24], beryllium [7], chromium [24, 25], molybdenum [24, 26], zirconium [24], hafnium [24, 27] and niobium [24, 28]. Many of these additions can introduce fine precipitates or dispersoids that resist grain-boundary sliding and retain high-temperature strength by resisting particle growth. Some elements such as boron can prevent intergranular decohesion at grain boundaries by preferential habitation [29].

Recent work shows that additions upto 10% Mo along with 1% TiB_2 in Fe–28% Al results in a decrease in grain size, an increase in the recrystallization

0022–2461/91 $03.00 + .12

TABLE I Properties of nickel, iron and titanium aluminides [19]

Alloy	Crystal structure	Critical ordering temperature, T_c (°C)	Melting point T_m (°C)	Material density (g cm^{-3})	Young's modulus (GPa)
Ni_3Al	LI2 (ordered fcc)	1390	1390	7.50	178.5
NiAl	B2 (ordered bcc)	1640	1640	5.86	294.2
Fe_3Al	DO_3 (ordered bcc)	540	1540	6.72	140.6
	B2 (ordered bcc)	760	1540		
FeAl	B2 (ordered bcc)	1250	1250	5.56	260.4
Ti_3Al	DO_{19} (ordered hcp)	1100	1600	4.2	144.7
TiAl	LI_0 (ordered tetra)	1460	1460	3.91	175.6
$TiAl_3$	DO_{22} (ordered tetra)	1350	1350	3.4	

temperature and also an increase in the DO_3 to B2 ordering transition temperature [26], all of these contributing towards better high-temperature strength and creep resistance. The ordered DO_3 structure is also reported to possess better high-cycle fatigue (HCF) resistance at elevated temperature in comparison to ordered B2 structure [30].

Apart from alloying, the introduction of fine grains through rapid solidification has also been attempted for improving ductility at ambient temperature. Both ribbons [31, 32] and powders [23] have shown enhanced ductility with alloy additions.

Of the various alloying elements mentioned above, boron has received a good deal of attention in view of having achieved dramatic success in the case of Ni_3Al [3–6]. However, results so far show that boron is not as effective in the case of Fe_3Al. In the Fe_3Al bcc-based ordered intermetallics, the lower-temperature ordered DO_3 structure shows a brittle cleavage fracture [33, 34]. The higher-temperature ordered B2-FeAl phase, in contrast, shows primarily intergranular fracture at ambient temperature [35, 36].

Regarding the phase diagram of Fe–Al, there has been a lack of agreement between the large number of earlier research reports [37–40], which stems primarily from the complication of higher-order transitions displayed in the system. Until recently, significant differences were reported in the phases formed. These were subsequently rationalized by the classic work of Allen and Cahn [41] on the basis of coherent and incoherent equilibrium diagrams. Fig. 1a shows the relevant portions of the Fe–Al diagrams due to Okamoto and Beck [39], Oki *et al.* [42] and Swann *et al.* [37]. Fig. 1b shows the rationalized diagram proposed by Allen and Cahn [41].

Recent reports indicate that ductility could be pushed to as high as 10% from a low value of 1% at ambient temperature and that tubes as well as sheets and castings could be fabricated successfully [43]. However, because of its strategic importance, the open literature still does not carry sufficient information about the chemistry and processing parameters that would usher in an immediate commercial use. Also, barring a few recent publications, one does not find systematic investigations throwing light on the role of alloy additions on the mechanical properties or phases formed.

The present investigation, which forms a part of a larger programme to develop Fe–Al materials for commercial exploitation, attempts to throw some light on

(i) the structural characteristics of Fe_3Al-based alloy made through conventional casting with and without microadditions;

(ii) some characteristics of alloys made by rapid solidification processing (RSP) with microadditions; and

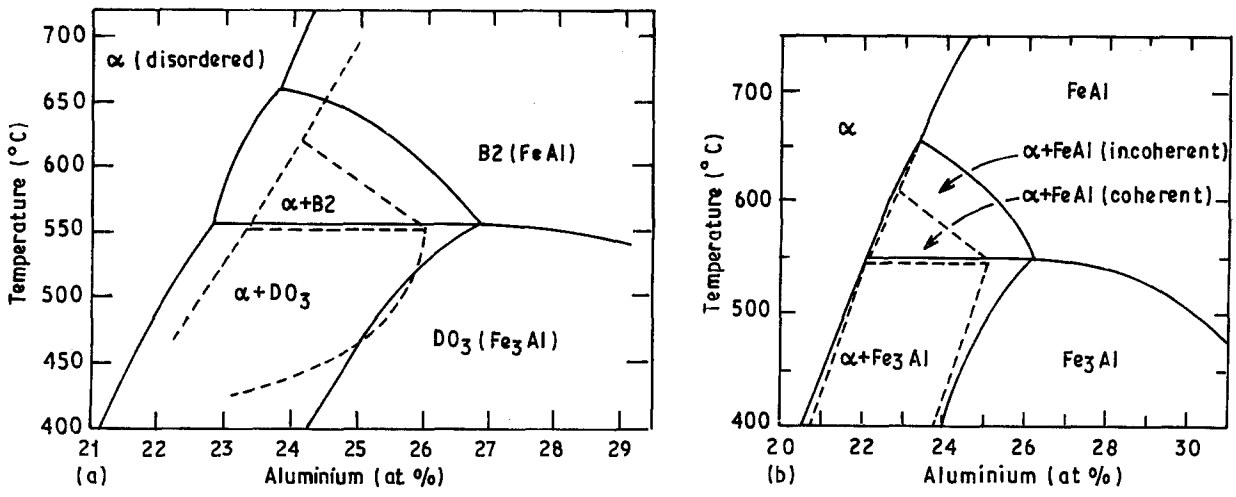

Figure 1 (a) (——) equilibrium [39] and (- - -) metastable [42] Fe–Al phase diagram [16]. (b) Superposition of the phase diagrams of (——) Okamoto and Beck [39] and (- - -) Swann *et al.* [41].

(iii) the basic workability of the material at high temperature and the tensile properties at room temperature.

2. Experimental procedure

2.1. Conventional casting

The alloys were cast in metal moulds from an air-induction melting furnace (Table II). The ingots were homogenized at 1100 °C for 48 h, forged and rolled at 900 °C repeatedly until maximum deformation (without cracking) was obtained. The rolled sheets were held at 900 °C and water-quenched (WQ) or air-cooled (AC).

2.2. Rapid solidification

Castings of modified alloys (with B + Ti) were remelted and melt-spun ribbons were produced in a laboratory-fabricated unit. Two sets of heat treatments were done. The ribbons were held at 500 °C for 2 h and furnace-cooled. Another set of ribbons was held at 570 °C for 3 min, 10 min or 5 h and water-quenched. The as-cast ribbons were pulverized in a ball mill and compacted manually, encapsulated in a mild steel capsule, forged and rolled at 900 °C.

2.3. Structural characterization and mechanical testing

Structural characterization was done using optical microscopy, transmission electron microscopy (TEM) as well as X-ray diffractometry (XRD). Thinning of samples for TEM was done using a twin jet polisher in a 5% perchloric acid–acetic acid bath. Microhardness was also measured on the samples.

For the forged Alloy C, electron probe microanalysis (EPMA) was done to determine the distribution of elements and the composition of inclusions.

Flat sub-size tensile specimens of length 100 mm were made from rolled sheets of Alloys C and D and tested in a Hounsfield Tensometer for UTS and percentage elongation.

The fractured surfaces of tensile specimens of Alloys C and D were examined in the scanning electron microscope for conventionally cast material.

3. Results

3.1. Conventional casting route

3.1.1. Cast and homogenized material

The microstructures show coarse columnar grains for Alloys A and C (Fig. 2a and b) and coarse equiaxed grains in (B + Ti)-modified Alloy D (Fig. 2c).

TABLE II Compositions of alloys prepared

Alloy designation	Composition (wt %)			
	Al	C	B	Ti
A	16.7	0.07	–	–
C	14.5	0.05	0.001	–
D	13.3	0.06	0.001	0.08

The average microhardness of alloys as shown in Table III corresponds to that of Fe_3Al compound. Table IV gives the available approximate microhardness values of Fe–Al intermetallic compounds [44]. XRD of Alloy A as shown in Fig. 3 and that for Alloy C show the presence of fundamental lines of $D0_3$ structure along with one set of superlattice lines, SL_1: (2 0 0), (2 2 2) and (4 2 0) but without the second set of superlattice lines, SL_2: (1 1 1), (3 1 1) and (3 3 1), which are exclusive to $D0_3$ order. Alloy D showed the presence of all lines with a lattice parameter of 0.579 nm. The presence or absence of SL_2 at all stages of these alloys as determined by XRD has also been reported in Table III.

3.1.2. Hot-forged material

The hot-forged structure shows fine equiaxed grains in all cases, as shown in Fig. 4, the finest being in modified alloys. XRD reveals one set of SL_1 lines in Alloy A and both sets in Alloy D. EPMA on Alloy C reveals that inclusions are mostly of aluminium oxides and sometimes of boron oxide.

3.1.3. Hot-rolled and heat-treated material

The equiaxed grains obtained on rolling, reheating and water-quenching (Fig. 5) are the finest in Alloy D (Fig. 5c). Further rolling causes grain growth. The average microhardness is higher in the as-rolled sheets and decreases on reheating and tends towards the reported Fe_3Al value.

The unmodified alloy could take a maximum deformation (reduction in thickness) of 65%, whereas boron- and (B + Ti)-modified alloys could be deformed by over 97% without cracking, finally leading to a 0.7 mm thick rolled sheet. The ductility of specimens of Alloys C and D was found to be 2.8 and 5%, respectively, compared with a reported value of less than 1% for unmodified alloys. The UTS of Alloys C and D was 686 and 863 MPa, respectively. The fractured surfaces viewed in the SEM show mostly cleavage fracture (a river pattern) in Alloy C (Fig. 6a) and a mixed fracture (both dimples and river patterns) in Alloy D (Fig. 6b).

3.2. RSP route

3.2.1. As-cast material

The microstructures show very fine equiaxed grains compared with the ingot structure. The wheel-side grains are finer than the air-side grain structure (Fig. 7), the finest being in Alloy D/wheel-side (Fig. 7c). The inclusions are more finely dispersed in ribbons compared with the ingot. A harder phase was observed in Alloy D which could be FeAl (Table V). XRD shows the presence of $D0_3$ order in both C and D alloys (Fig. 8).

3.2.2. Heat-treated ribbons

The ribbons held at 500 °C, i.e. in the (α + $D0_3$) region according to Allen and Cahn's diagram (Fig. 1b) and

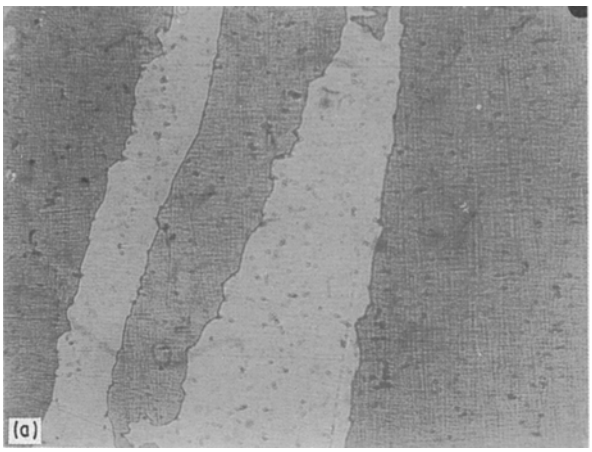

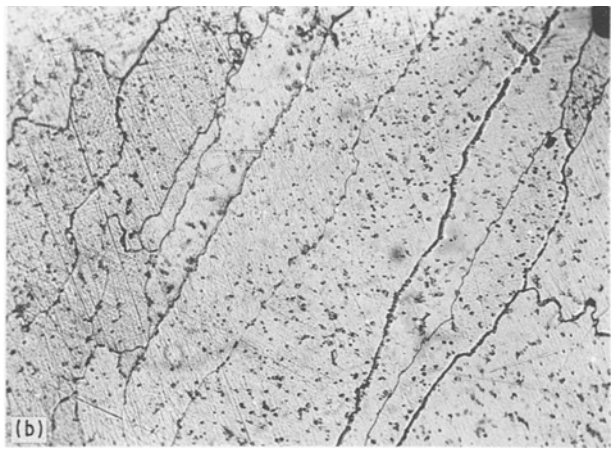

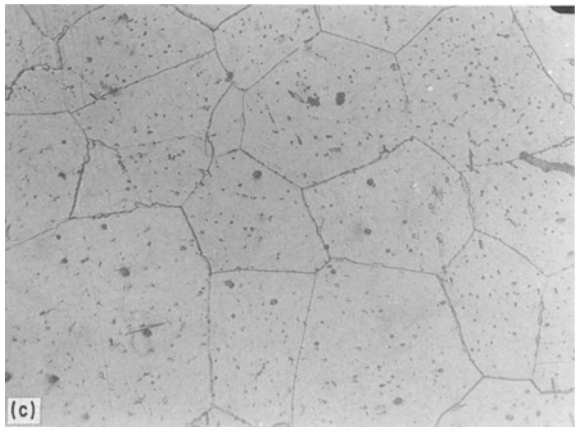

Figure 2 Optical microstructures of as-cast ingots. (a) Unmodified and (b) boron-modified alloys show coarse columnar grains; (c) (B + Ti)-modified alloy shows coarse equiaxed grains. × 100.

furnace-cooled (FC) showed complete $D0_3$ order by XRD (Table V). The microhardness of ribbons held at 570 °C and water-quenched indicates a combination of Fe_3Al and a harder phase (which could be FeAl). The first set of superlattice lines was identified, while the second set SL_2 was absent. Thus holding at 570 °C in the (α + B2) region even for 3 min and WQ appears to be sufficient for partly suppressing $D0_3$ order, partly in contrast to the as-RSP structures.

TEM micrographs show the presence of antiphase domain boundaries (APB) both in as-cast (Fig. 9a) and heated (570 °/3 min/WQ) samples (Fig. 9b), confirming ordering in these compounds. The selected-area diffraction pattern (SAD) of as-cast ribbon is shown in Fig. 9c along with the indexed diagram showing superlattice points such as (1 1 1) in the $D0_3$ lattice (Fig. 9d).

3.2.3. Ribbons pulverized and hot-worked

The microstructure shows that bonding has taken place, although there still are some regions of discontinuity (Fig. 10). The microhardness is 354 VPN and XRD shows the presence of $D0_3$ order.

4. Discussion

It may be observed from the microstructure of conventionally cast alloys that, with modification of the base alloys, more particularly with (B + Ti), there is a refinement in structure as well as a change-over from columnar to equiaxed. There may be a synergistic effect of boron and titanium in enhancing the rate of nucleation, although there is also a variation in aluminium in these alloys. The influence of a small variation in aluminium on a possible synergistic effect between boron and titanium would be considered as low. However, no direct literature-reference is available on this subject. As is evident, these alloys show an encouraging response to hot forging – the grain refinement due to dynamic recrystallization is clear. However,

TABLE III Average microhardness and XRD data for alloys along rolling direction

Condition	Alloy					
	Unmodified (A)		Boron-modified (C)		(B + Ti)-modified (D)	
	μH(VPN)	SL_2 (*hkl*)	μH(VPN)	SL_2 (*hkl*)	μH(VPN)	SL_2 (*hkl*)
As-cast	302	No	333	No	368	Yes (1 1 1)
Forged	320	No	383	No	390	Yes (1 1 1, 3 1 1)
Forged/rolled	432	No	518	No	442	Yes (1 1 1)
Forged/rolled/WQ	363	No	357	No	380	No
Forged/rolled/AC	326	Yes (1 1 1)	441	Yes (1 1 1)	390	Yes (1 1 1, 3 1 1, 3 3 1)
Further rolled	NA	–	427	No	453	No
Rolled/WQ	NA	–	–	–	350	Yes (1 1 1)
Rolled/AC	NA	–	416	Yes (1 1 1)	385	Yes (1 1 1)

TABLE IV Approximate hardness values of Fe–Al Intermetallics [44]

Phase	Approximate hardness ($kg\,mm^{-2}$)
Fe_3Al	350
FeAl	640
$FeAl_2$	1030
Fe_2Al_5	820
$FeAl_3$	990
Fe_2Al_7	1080

there is a perceptible grain-growth during the subsequent hot rolling of the forged plates. This broadly indicates that the amounts of titanium and boron present in the material are not very effective in checking the grain-growth. It may be observed that the levels of titanium and boron additions in the alloys of previous investigations [23, 31, 32] are much higher.

The microstructures of rapidly solidified alloys show an equiaxed structure in the as-cast condition and the grain size is also considerably finer. These are essentially predicted effects of rapid solidification. There are some references in the literature where rapid solidification has been adopted and evidence of cellular or dendritic structure has been reported [23] along with TiB_2 particles in the intercellular regions. In these cases, however, cooling rates greater than $10^5\,^{\circ}C\,sec^{-1}$ (with centrifugal atomization) were employed which are higher than in the present case. Further, in some of the previous investigations (45) carbon (1.7 to 2.1 wt %) was deliberately added and a non-equilibrium ductile fcc phase was observed.

TEM of the RSP samples presents some interesting results. Both the as-cast as well as heat-treated (570 °/WQ) samples show the presence of APBs, and there is hardly any difference in the sizes of the APBs in these two cases. The XRD data, however, show the absence of some superlattice lines in the 570 °/WQ case. Now, the designation of the superlattice and fundamental lines has been dealt with comprehensively by Fortnum and Mikkola [46], and in the present work a similar scheme was followed. The Fe_3Al structure (cubic) consists of fundamental lines when h, k, and l are even and $(h + k + l)/2$ is also even, as in 2 2 0, 4 0 0 and 4 2 2. The first set of superlattice reflections SL_1 has h, k and l all even and $(h + k + l)/2$ odd, e.g. 2 0 0, 2 2 2, 4 2 0. Such reflections correspond to an ordered B2 compound and also to $D0_3$. Lastly, when h, k and l are all odd (as in 1 1 1, 3 1 1, 3 3 1) these lines correspond to superlattice lines SL_2 for $D0_3$ order alone. The ratios of integrated intensities of the various lines, however, did not concur with the theoretical values, particularly in the conventionally cast condition. The large grain-size of the structure is believed to be responsible for this. Since the size of grains here is larger than the X-ray beam-size, the contribution of texture is considered to be low as far as observed anomalous line-intensities are concerned.

The high-temperature workability of the alloys seems to be very good. It is known [45] that the $D0_3$ to B_2 transition results in an appreciable fall in yield and tensile stresses. This change may contribute to the enhanced hot workability. Ambient-temperature tensile test results are also encouraging, with elongation around 5% for (Ti + B) grades. There are reports [22–25] to show that by alloy addition, the ductility did improve; again, the earlier investigations (e.g. [23])

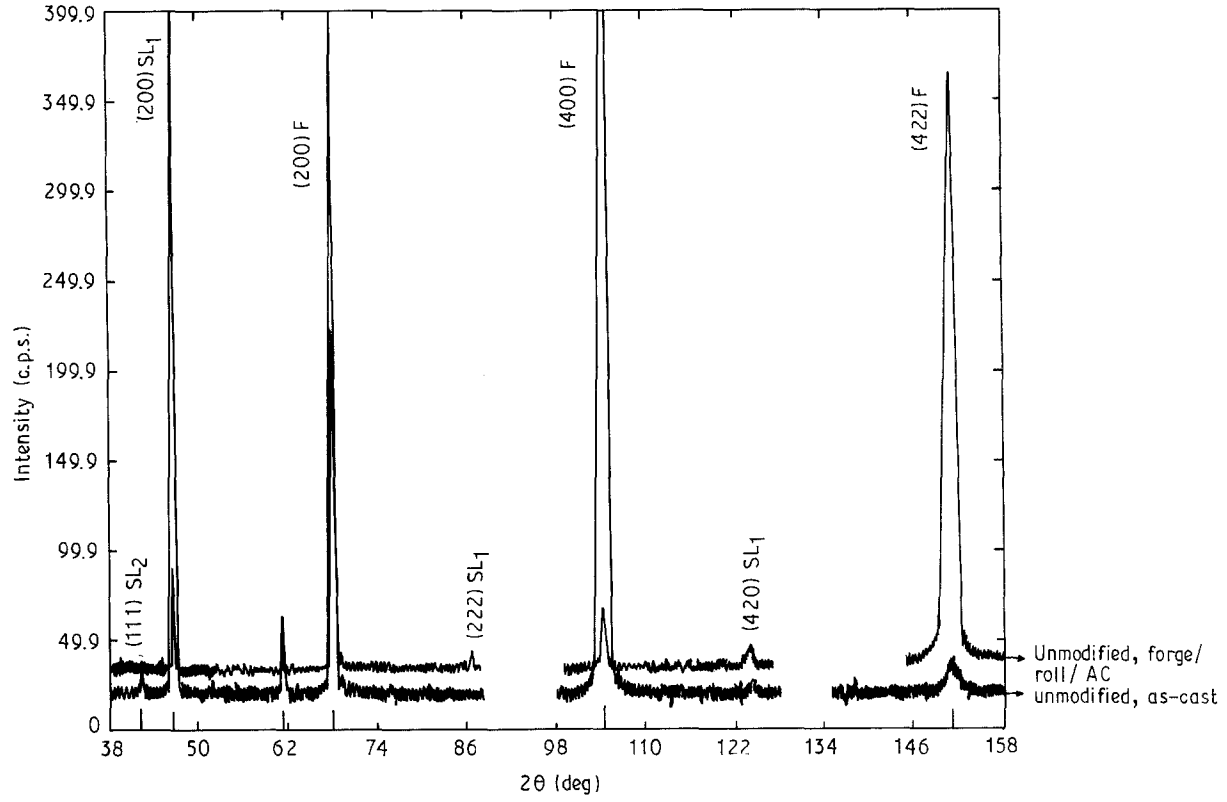

Figure 3 XRD of unmodified Fe_3Al alloy ingot in as-cast and forged/rolled/AC conditions.

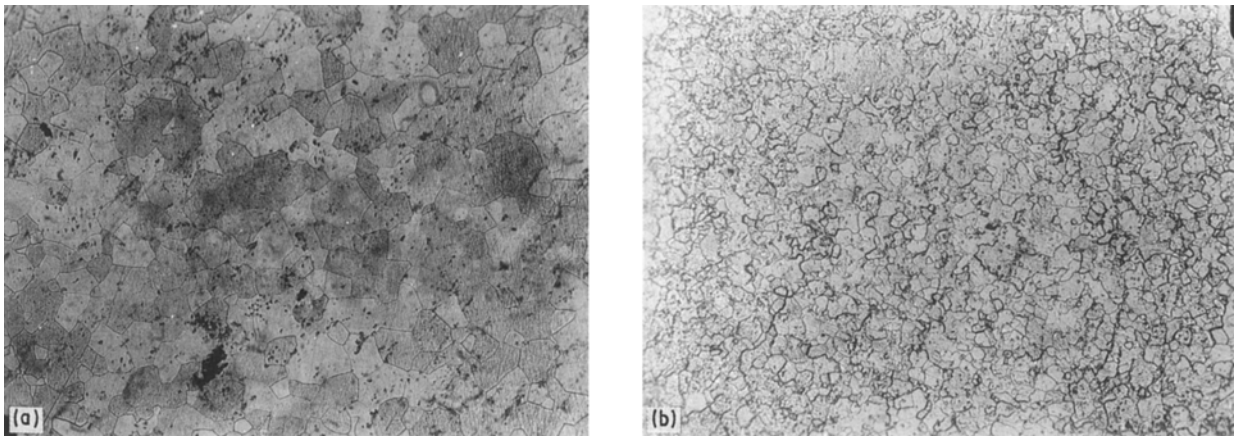

Figure 4 Optical microstructures in As-forged condition shows fine equiaxed grains in (a) unmodified, (b) boron-modified and (c) (B + Ti)-modified alloys. × 100.

primarily operated at a higher level of alloy additions. The SEM results for fractured samples did confirm the good ductility through the presence of dimples.

5. Conclusions

The present work on Fe_3Al, though preliminary in nature, did indicate the following:

1. Air-melting and micro-additions such as boron and titanium to Fe_3Al-based alloys bring about changes in the microstructure from columnar to equiaxed in the as-cast condition.
2. The addition of boron and titanium makes these alloys amenable to hot working. 97% reduction was achieved in these alloys (leading to a 0.7 mm thick rolled sheet) compared with 65% in unmodified alloy, and a greater workability is also achieved.
3. Rapid solidification induces a fine grain size and the material shows good bonding characteristics on compacting and hot working.
4. The formation of ordered intermetallic phases takes place too rapidly to be suppressed by rapid solidification.

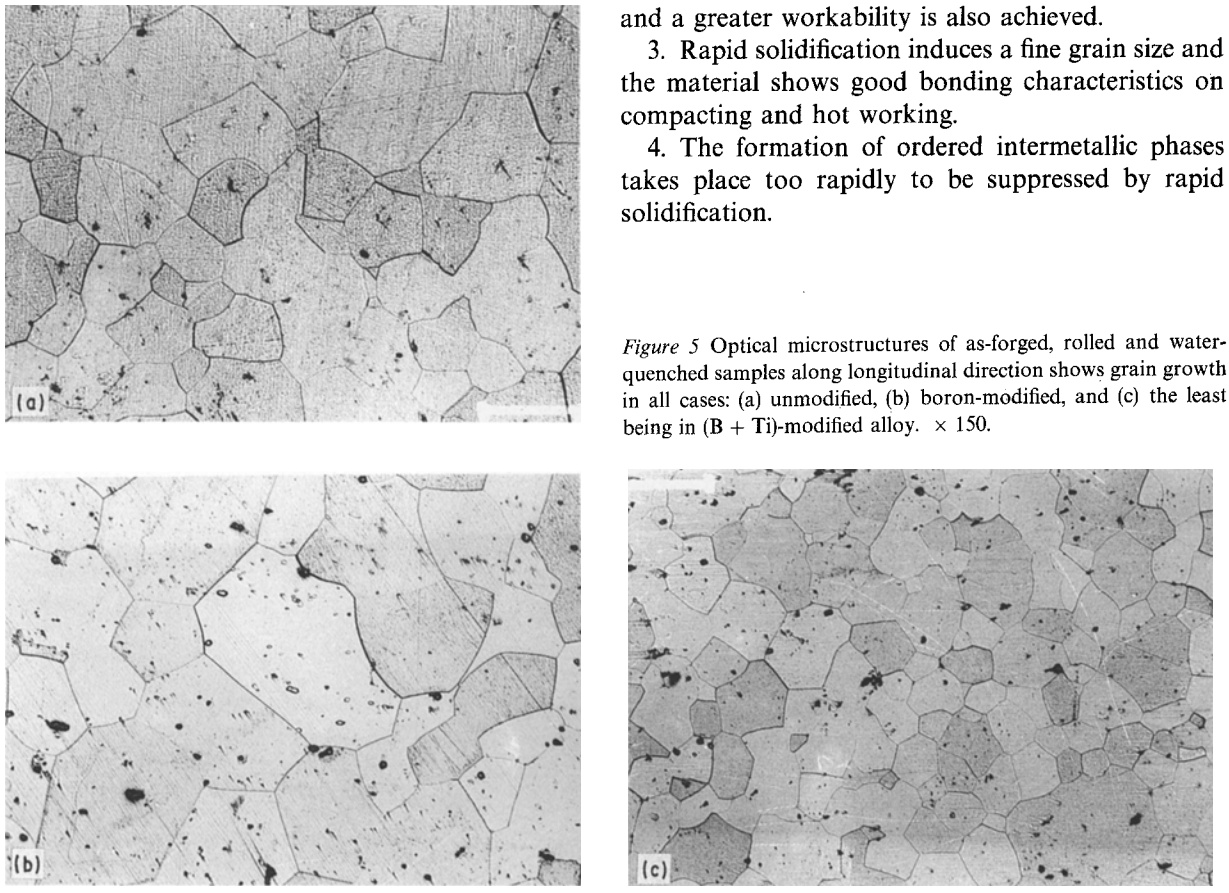

Figure 5 Optical microstructures of as-forged, rolled and water-quenched samples along longitudinal direction shows grain growth in all cases: (a) unmodified, (b) boron-modified, and (c) the least being in (B + Ti)-modified alloy. × 150.

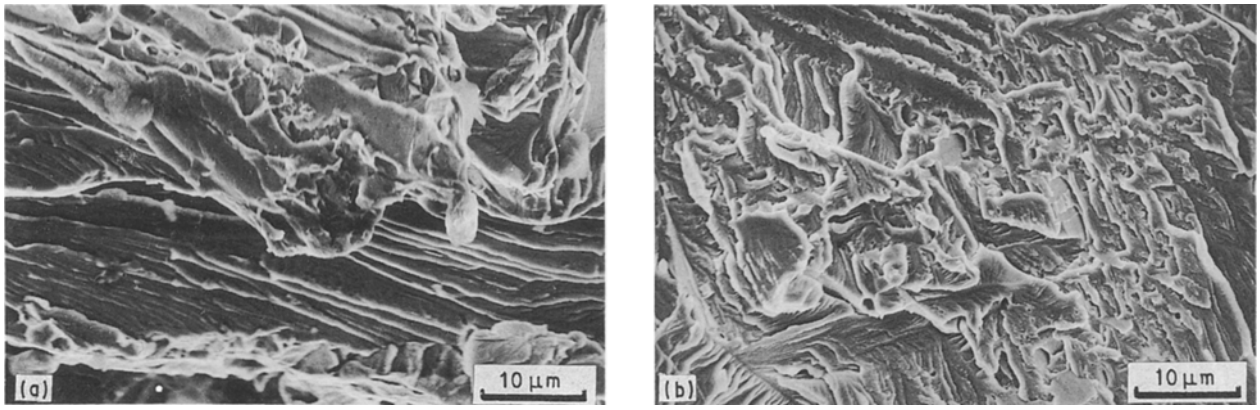

Figure 6 SEM photomicrographs of fractured tensile specimens from forged, rolled sheets show cleavage fracture (river pattern) in (a) boron-modified alloy and (b) mixed fracture (both dimples and river pattern) in (B + Ti)-modified alloy.

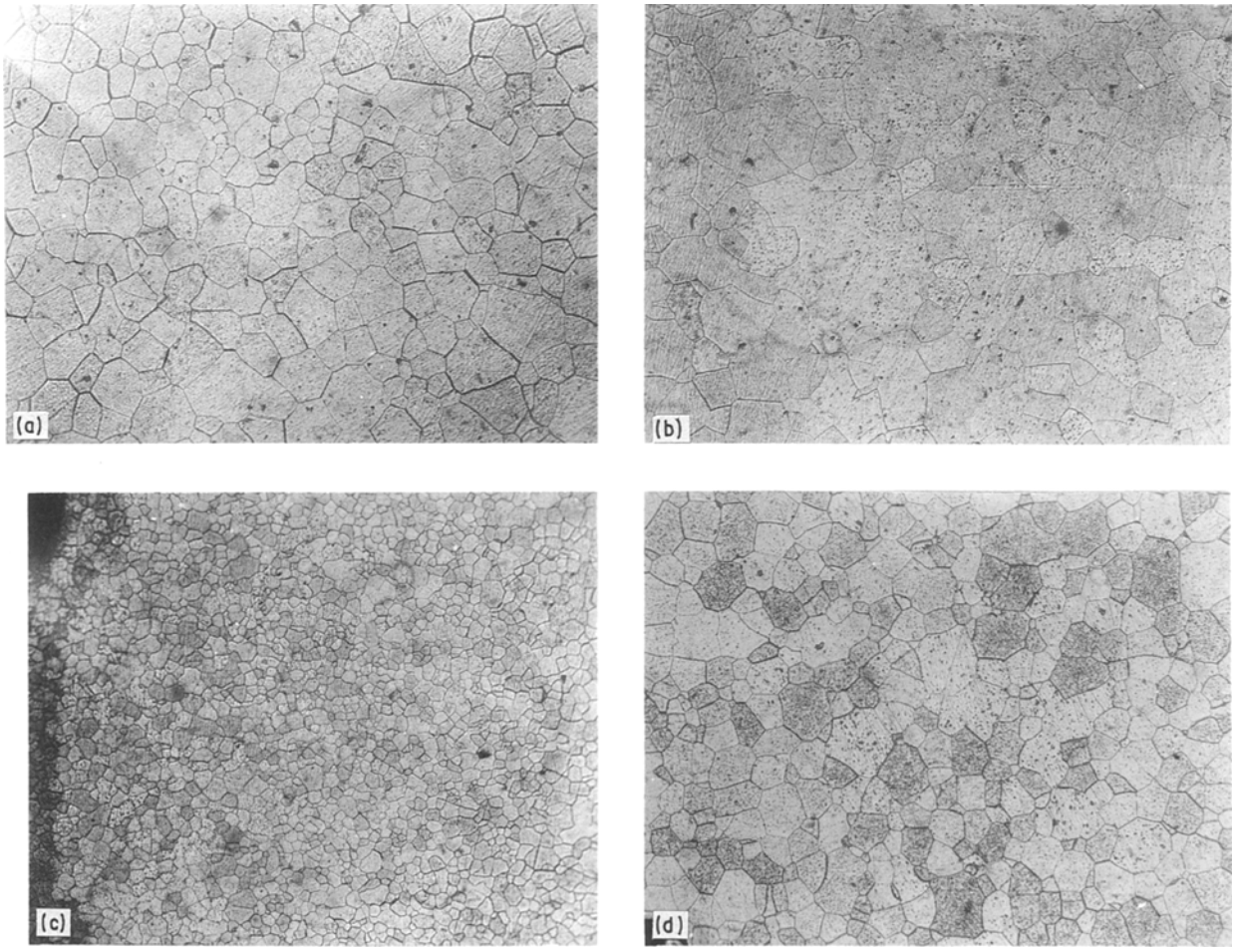

Figure 7 Optical microstructures of rapidly solidified ribbons of boron-modified alloy (a) wheel-side and (b) air-side, and (B + Ti)-modified alloy, (c) wheel-side and (d) air-side. The wheel-side shows finer grains in both compared to the air-side, the finest grains being in (B + Ti)-modified alloy (wheel-side). × 100.

TABLE V Average microhardness and XRD data for RSP alloys

Condition	Alloy			
	Boron-modified (C)		(B + Ti)-modified (D)	
	Av. μH (VPN)	SL_2 (*h k l*)	Av. μH (VPN)	SL_2 (*h k l*)
As-cast	350	Yes (1 1 1)	395 + harder phase	Yes (1 1 1)
500°/2 h/FC	–	–	–	Yes (1 1 1, 3 1 1, 3 3 1)
570 °/10 min/WQ	–	–	–	No
570 °/5 h/WQ	–	–	366 + harder phase	No
Powder/compacted/forged/rolled	–	–	354	Yes (1 1 1)

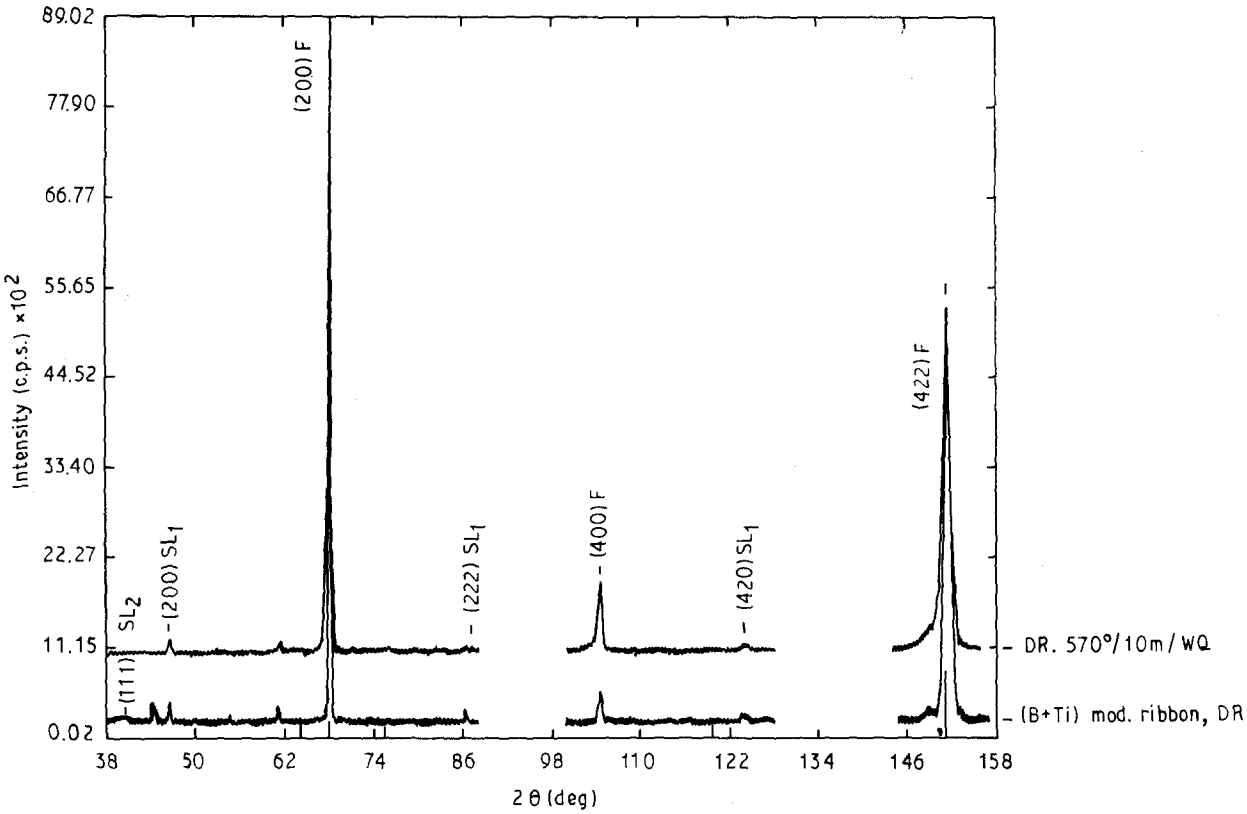

Figure 8 XRD of (B + Ti)-modified alloy ribbon in as-cast and 570 °/10 min/WQ condition shows the presence of both sets of SL lines in as-cast and only SL_1 in the latter.

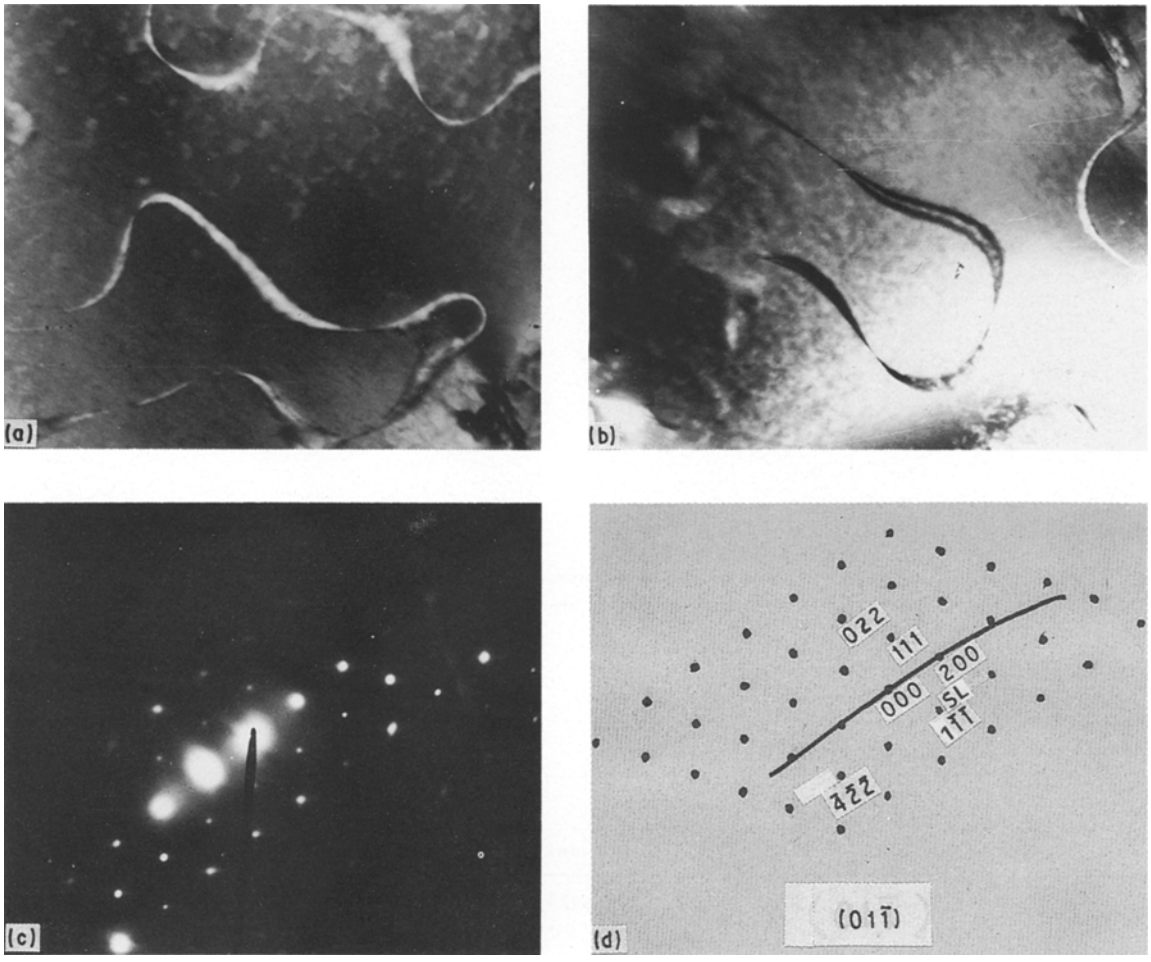

Figure 9 TEM photomicrographs of (B + Ti)-modified alloy ribbon in (a) as-cast condition, × 33 000 and (b) 570 °/3 min/WQ condition showing APB ordering, × 42 000. (c) The selected-area diffraction pattern of as-cast ribbon is indexed in (d).

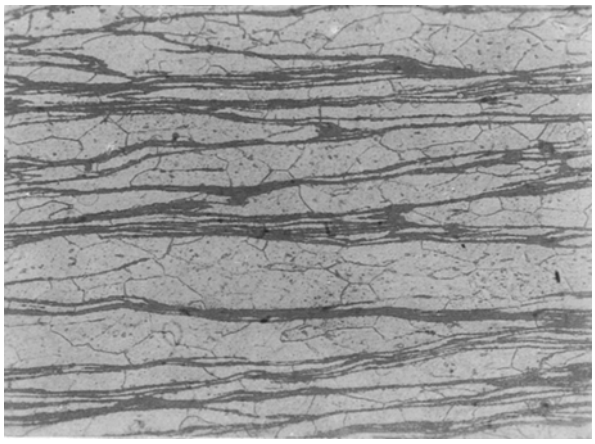

Figure 10 Optical microstructure of (B + Ti)-modified ribbons pulverized, encapsulated, forged and rolled in transverse section. × 200.

Acknowledgements

The authors wish to express their gratitude to Professor S. Banerjee, Director, National Metallurgical Laboratory, Jamshedpur for encouragement and permission to publish this work. The authors also record their thanks to Sri. S. Das for the TEM work.

References

1. J. O. STIEGLER and C. T. LIU, "Encyclopaedia of Material Sciences and Engineering", Supplementary Vol. 1, edited by R. W. Cahn (Pergamon, New York, 1988) p. 3.
2. T. OGURA, S. HAMADA, T. MASUMOTO and O. IZUMI, *Met. Trans. A* **16A** (1985) 441.
3. I. BAKER, B. HUANG and E. M. SCHULSON, *Acta Metall.* **36** (1988) 493.
4. P. S. KHADIKAR, K. VEDULA and B. S. SHABEL, *Met. Trans. A* **18A** (1987) 425.
5. *Idem, ibid.* **18A** (1987) 1995.
6. A. I. TAUB, S. C. HUANG and K. M. CHANG, *ibid.* **15A** (1984) 399.
7. T. TAKASUGI, N. MASAHASHI and O. IZUMI, *Scripta Metall.* **20** (1986) 1317.
8. I. BAKER, J. A. HORTON and E. M. SCHULSON, *J. Mater. Sci.* **21** (1986) 3297.
9. D. J. GAYDOSH, R. W. JECH and R. H. TITRAN, *ibid.* **4** (1986) 138.
10. T. C. CHOU and Y. T. CHOU, *Mater. Lett.* **4** (1986) 423.
11. F. H. FROES and R. G. ROWE, *Mater. Res. Soc. Symp. Proc.* **58** (1986) 309.
12. R. G. ROWE, A. I. TAUB and F. H. FROES, "Rapid Solidification Processing: Principles and Technologies, IV", edited by R. Meharbian (Claitor's Publishing Division, Louisiana, Santa Barbara, 1986).
13. D. J. GAYDOSH and M. A. CRIMP, *MRS Symp. Proc.* **39** (Materials Research Society, 1985) 429.
14. N. S. STOLLOF, *Int. Metals Rev.* **29** (1984) 123.
15. A. LAWLEY, in "Intermetallic Compounds", edited by J. H. Westbrook (Wiley, New York, 1967) p. 464.
16. H. INOUYE, *Mater. Res. Soc. Symp. Proc.* **39** (1985) 255.
17. N. S. STOLLOF and R. G. DAVIES, *Acta Metall.* **12** (1964) 473.
18. A. LAWLEY, E. A. VIDOZ and R. W. CAHN, *ibid.* **9** (1961) 287.
19. R. A. RICKS, A. J. PORTER and R. C. ECOB, *ibid.* **31** (1983) 43.
20. R. RAY, V. PANCHANATHAN and S. ISSEROW, *J. Metals* June (1983) 30.
21. J. E. WITTIG, E. VOGT, R. MÖLLER and G. FROMMEYER, *Scripta Metall.* **21** (1987) 721.
22. M. A. CRIMP and K. VEDULA, *Mater. Sci. Engng* **78** (1986) 193.
23. E. R. SLAUGHTER and S. K. DAS, "Rapid Solidification Processing: Principles and Technologies II", edited by R. Mehrabian, B. H. Kear and M. Cohen (Claitor's, Baton Rouge, Louisiana, 1980) p. 354.
24. R. H. TITRAN, K. M. VEDULA and G. G. ANDERSON, *Mater. Res. Soc. Symp. Proc.* **39** (1985) 309.
25. C. G. McKAMEY and J. A. HORTON, *Met. Trans. A* **20A** (1989) 751.
26. C. G. McKAMEY, J. A. HORTON and C. T. LIU, *Scripta Metall.* **22** (1988) 1679.
27. S. TANIGUCHI, T. SHIBATA and H. TSURUOKA, *Trans. Jpn Inst. Metals* **28** (1987) 788.
28. K. WAMBACH, J. PETERS and H. J. GRABKE, *Mater. Sci. Engng* **88** (1987) 205.
29. G. B. OLSON and R. G. BOURDEAU in Proceedings of Conference, "Rapidly Solidified Crystalline Alloys" Morristown, New Jersey, May 1985, edited by S. K. Das, B. H. Kear and C. M. Adams (Metals Society, AIME) p. 185.
30. G. E. FUCHS and N. S. STOLOFF, *Acta Metall.* **36** (1988) 1381.
31. C. C. KOCH, *Mater. Res. Soc. Symp. Proc.* **39** (1985) 397.
32. *Idem, Int. Mater. Rev.* **33** (1988) 201.
33. M. G. MENDIRATTA, S. K. EHLERS, D. K. CHATTERJEE and H. A. LIPSITT, *Met. Trans. A* **18A** (1987) 283.
34. W. R. KERR, *ibid.* **17A** (1986) 2298.
35. M. J. MARCINKOWSKI, M. E. TAYLOR and F. X. KAYSER, *J. Mater. Sci.* **19** (1975) 406.
36. M. J. MARCINKOWSKI and J. LARSEN, *Met. Trans.* **1** (1970) 1034.
37. P. R. SWANN, W. R. DUFF and R. M. FISHER, *Trans. Met. Soc. AIME* **245** (1969) 851.
38. H. WARLIMONT and G. LUTJERING, *Acta Metall.* **12** (1964) 1460.
39. H. OKAMOTO and P. A. BECK, *Met. Trans.* **2** (1971) 569.
40. O. KUBASCHEWSKI, "Iron-Binary Phase Diagrams" (Springer, Berlin, 1982) p. 5.
41. S. M. ALLEN and J. W. CAHN, *Acta Metall.* **23** (1975) 1017.
42. K. OKI, M. HASAKA and T. EGUCHI, *Jap. J. Appl. Phys.* **12** (1973) 1522.
43. *Adv. Mater. Processes Metal Progr.* **12** (1988) 26.
44. L. N. LARIKOV, V. M. FAL'CHENKO, D. F. POLISCHUK, V. R. RYABOV and A. V. LOZOVSKAYA, *Prot. Coatings Metals* **3** (1971) 66.
45. A. INOUE, T. MINEMURA, A. KITAMURA and T. MASUMOTA, *Met. Trans. A* **12A** (1981) 1041.
46. R. T. FORTNUM and D. E. MIKKOLA, *Mater. Sci. Engng* **91** (1987) 223.

Received 8 February
and accepted 6 June 1990